Chaotic edge density fluctuations in the Alcator C-Mod tokamak

Z. Zhu,[1, a)] A. E. White,[2] T. A. Carter,[1] S. G. Baek,[2] and J. L. Terry[2]
[1)] *Department of Physics and Astronomy, University of California, Los Angeles, CA 90095, USA*
[2)] *MIT Plasma Science and Fusion Center, Cambridge, MA 02139, USA*

(Dated: 21 February 2017)

Analysis of the time series obtained with the O-Mode reflectometer (Rhodes *et al* 1997 *Plasma Phys. and Control. Fusion* **40** (1998) 493-510) and the gas puff imaging (Cziegler, I. *et al* 2010 *Phys. of Plasmas* **17**, No. 5 (2010) 056120) systems on the Alcator C-Mod tokamak reveals that the turbulent edge density fluctuations are chaotic. Supporting evidence for this conclusion includes: the observation of exponential power spectra (which is associated with Lorentzian-shaped pulses in the time series), the population of the corresponding Bandt-Pompe probability distributions (Bandt and Pompe 2002 *Phys. Rev. Lett.* **88** 174102), and the location of the signal on the complexity-entropy plane (C-H plane) (Rosso *et al* 2007 *Phys. Rev. Lett.* **99**, 154102 (2007)). The classification of edge turbulence as chaotic opens the door for further work to understand the underlying process and the impact on turbulent transport.

Keywords: turbulence, chaos, fusion, tokamaks

arXiv:1612.04046v3 [physics.plasm-ph] 19 Feb 2017

I. INTRODUCTION

magnetic-confined plasmas; understanding the nature of this turbulence and the associated transport is therefore of great importance. The transport associated with plasma fluctuations, and the ability to predict that transport, may be affected by the underlying nature of fluctuations, that is, whether the process generating the fluctuations is chaotic or stochastic. Stochastic processes generate fluctuations with random time series, and have trajectories that can sample all of phase space. In the presence of stochastic fluctuations, transport by random walk diffusion is expected. Chaotic processes, on the other hand, are deterministic and can be generated by the interaction of a few coupled modes (a minimum of two). These processes live in restricted areas of phase space (e.g. on attractors).[1] As such, a random walk diffusion model is unlikely to be a valid description of transport arising from such a process. In tokamak plasmas, there is a great deal of evidence that core transport is well described by diffusive models,[2] but there is also evidence that the transport may be in some instances non-diffusive.[3] Turbulence in the edge and Scrape-Off-Layer (SOL) of tokamaks can be bursty, with intermittent "blobs" leading to non-diffusive transport.[4–6]

In this work, analysis of data from two standard turbulence diagnostics, the reflectometer and the gas puff imaging (GPI) system, was performed, seeking to indicate the nature of edge turbulence in the Alcator C-Mod tokamak. The multi-channel reflectometer provides simultaneous localized measurement of density fluctuations at several radial positions covering the core to the edge of the plasma with excellent temporal resolution,[7] whereas the GPI provides measurement of emission fluctuations within a 2D grid (radial and poloidal) that spans a $\sim 3.4 \times 3.8$ cm region near the last closed flux surface (LCFS) on the low-field-side. The spatial resolution is roughly 5 mm and the temporal resolution is 1 MHz. The majority of the analysis reported in this paper is on the time series obtained by the reflectometer in the low confinement regime (L-mode) plasmas. A comparison between reflectometry and

[a)] Electronic mail: zhuziyan@ucla.edu

the GPI results and an initial analysis of fluctuations in the high energy confinement regime (H-mode) and improved energy confinement regime (I-mode) plasmas are also included.

Three analysis techniques are used on the time signals in order to identify whether the underlying process is stochastic or chaotic. These include evaluating: the fluctuation power spectra,[1] the Bandt-Pompe (BP) probability distribution,[8] and the complexity-entropy (C-H) plane.[9] Chaotic processes have been shown to generate power spectra that are exponential; these exponential spectra are associated with Lorentzian pulses in the time series signal.[1] The BP probability distribution provides information on the structure of the time series signal by evaluating the distribution of amplitude orderings in the signal. The C-H plane analysis makes use of the BP probability distribution to classify the nature of the signal based on the so-called complexity and the BP entropy. The BP probability distribution and the C-H plane analysis have been successfully applied to analyze a number of time series including financial data,[10,11] mammal neural activities,[12] edge density fluctuations in tokamaks,[13,14], and MHD turbulence.[15] The results of the application of these three techniques indicate that the edge density fluctuations in L-mode, H-mode and I-mode plasmas in the Alcator C-Mod tokamak are chaotic. Similar chaotic edge density fluctuations were observed in a wide range of plasma devices of different geometries, such as in the DIII-D tokamak,[13] the TJ-K stellarator[16] and the Large Plasma Device.[17,18]

This paper is organized as follows: Sec. II briefly introduces the experimental device and discusses the two diagnostics (the O-mode reflectometery and the GPI) used in the experiments. Section III introduces the theoretical background of this study and the three main techniques used to distinguish between chaotic and stochastic signals. Section IV presents analysis of the experimental data using the techniques introduced in section III. Section V discusses the findings and presents conclusions.

II. EXPERIMENTAL SETUP

The experiments presented here were performed in the compact, high-field Alcator C-Mod tokamak [19]. The device has major radius $R = 0.67$m, minor radius $a = 0.22$m. In this work, a total of 61 shots are analyzed. A wide range of parameters and conditions are included in these shots: the toroidal magnetic field B_{T} ranges from 2.7 to 8 T; plasma current I_{p} ranges from 0.5 to 1.2 MA; the line averaged density ranges from 0.5 to $1 \cdot 10^{20}\mathrm{m}^{-3}$; the edge safety factor q95 ranges from 3 to 7; and the RF heating power P_{RF} ranges from 0.6 to 4.5 MW. Different confinement regimes were studied: low-energy confinement regime (L-mode), the high energy confinement regime (H-mode) and improved-energy confinement regime (I-mode). Some Ohmic plasmas (without RF heating) are also included. In each shot, 20 ms temporal signals were chosen based on the radial density profile measured by Thomson scattering diagnostics,[20] with the assumption that there is no significant change in the density profile within 20 ms.

The first diagnostic discussed in this work is the multi-channel O-Mode reflectometer.[21] Signals $S(t)$ collected by the reflectometer are complex and are composed of an amplitude component $E(t)$ and a phase component $\phi(t)$, $S(t) = E(t)\ e^{i\phi(t)}$. The real part of a signal is referred as the inphase, $S_{\mathrm{re}} = \mathrm{Re}[E(t)\ e^{i\phi(t)}]$, and the imaginary part is referred as the quadrature, $S_{\mathrm{im}} = \mathrm{Im}[E(t)\ e^{i\phi(t)}]$.[7] A total of 5 reflectometer channels was analyzed, giving measurements at a range of radial positions. The frequencies of the 5 channels are: 50 GHz, 60 GHz, 75 GHz, 88 GHz, and 112 GHz, with the cutoff density ranging from $0.3 - 1.5 \cdot 10^{20}\mathrm{cm}^{-3}$. Advantages of reflectometry include its high temporal resolution and capability of localized measurements. However, it is difficult to extract absolute fluctuation levels from reflectometer signals and the radial position of the measurement is not fixed in space, but varies with plasma density. The measurement position can be tracked during a shot by comparing the cutoff frequency with the density profile measured by a Thomson scattering diagnostic.[20]

The gas puff imaging (GPI) was also employed to measure turbulent edge fluctuations.[4,5,22] Helium gas is puffed locally into the Scrape-Off Layer, and HeI line emission

(587.6 nm) is monitored along sightlines that cross the puff region toroidally. Since the line emission is due to electron-impact excitation by the local plasma, the emissivity is a function of both n_e and T_e and responds to fluctuations in those plasma quantities. The emission rate can be parameterized as S (photon $\cdot$ s^{-1} $\cdot$ cm^{-3}) $\propto (n_e)^{\alpha} \cdot (T_e)^{\beta}$, where α and β depend on the time-averaged local quantities n_e and T_e.[23]. The GPI provides a 2D image of the normalized emission in the radial and poloidal directions.[23] Unlike reflectometry, the exact spatial positions of GPI-measured fluctuations are fixed by the viewing optics. In this study, GPI signals were located at radial positions ranging from roughly 1.5 cm inside the LCFS to 1.5 cm outside the LCFS at single height that is 2.4 cm below the outboard mid-plane. The reflectometry and GPI measurement were separated by 18 degrees toroidally. When we compare the results from the two, we do so by EFIT mapping[24] them to the same flux surface and use signals taken during the same time period. Both diagnostics were sampled at 2MS/s.

III. IDENTIFYING CHAOTIC VS. STOCHASTIC SIGNALS

Although chaotic and stochastic signals have distinct origins, they can be difficult to distinguish due to their similarities: both will give rise to time series that have broadband power spectra and seemingly random behavior.[9] This section introduces the three analysis tools to distinguish time series generated by chaotic and stochastic processes: (1) the shape of the power spectra, (2) the population of Bandt-Pompe (BP) probability distributions, and (3) the corresponding complexity-entropy (C-H) plane.

A. Power spectra and corresponding time series

It has been established by researchers in different disciplines since the 1980s that an intrinsic characteristic of deterministic chaos is the exponential power spectrum; i.e: $P(\omega) \propto \exp(-2\omega\tau)$, whereas stochastic processes are associated with power law spectra.[25–27] Although both chaotic and stochastic processes have broadband power spectra, exponential chaotic spectra can be formed by a small number of coupled modes. Such exponential power spectra correspond to Lorentzian shaped pulses in the time signals (eqn. 1).

$$L(t) = \frac{A}{\tau^2 + (t - t_0)^2} \tag{1}$$

In Eqn. 1, τ is referred to as the pulse width, which is the half width at half maximum; t_0 is the center of the pulse, and A is a normalization constant. Lorentzian-shaped pulses in time are produced by particle motions in the vicinity of the separatrix boundaries of elliptical regions in flow fields, or more generally, near the limit cycles of attractors in nonlinear dynamical models.[1] The pulse width is determined by the imaginary part of the eigenvalues of the Jacobian of the flow fields, which is essentially the angular frequency of each trajectory around the attractor. In general, the flow fields are associated with Lorentzian bifurcation transports scalar quantities, and in two-dimensional bifurcation, if a scalar quantity has a linear gradient in the y-direction (such as density and temperature gradients in magnetic-confined fusion devices), a Lorentzian shape in the y component of the potential field leads to the Lorentzian-shaped pulses in the trajectories.[1]

The power spectrum for a series of n Lorentzian pulses is then as follows,

$$\tilde{P}(\omega) \propto \sum_n e^{-2\omega\tau_n} \tag{2}$$

Therefore, if a temporal signal has a series of Lorentzian pulses with a well-defined pulse width, one should expect an exponential power spectrum, which exhibits a linear shape

on a semi-log scale. In this way, a broadband power spectrum can be formed by a low-dimensional chaotic process where a single time scale defines the dynamics. This is possible with a minimum of two interacting modes (the trajectory of particles in the potential fields of the two modes is chaotic).[1] The slope of a Lorentzian power spectrum on a semi-log scale is $-2\omega\tau = -4\pi\tau f$ (with the assumption of a single pulse width in the time history). Then, the value of τ can be found by fitting the slope of the spectrum on the semi-log scale:

$$\tau = -\frac{\text{slope}}{4\pi} \tag{3}$$

A complex time signal is constructed from the measurements of the amplitude and the phase of the reflected signal associated with the reflectometer diagnostic. The Fourier transform of a complex time signal has both negative and positive frequencies. In this work, the slope is fitted only for the positive frequencies since all presented spectra are roughly symmetric about the zero frequency. However, the GPI power spectra presented only have positive frequencies because GPI signals measure a single quantity (light fluctuation amplitude) and do not contain phase information, and thus were compared with real amplitude spectra from the reflectometer.

B. Bandt-Pompe probability and complexity-entropy plane

Stochastic and chaotic processes are distinct in the phase space that the time signals have access to and therefore in the structure of the generated time signals. Two techniques to distinguish the structures generated by chaotic and stochastic processes are the Bandt-Pompe (BP) probability distribution and the complexity-entropy (C-H) plane. The BP probability quantifies the frequency of occurrence of structure in time signals by using permutations of the ordering of the amplitudes of consecutive values, at evenly separated discrete points.[8] To compute the BP probability, an "embedding space" with dimension d is used. So-called "d-tuples" are generated by taking d consecutive points in the time signal and ordering them from largest amplitude to smallest. For example at time points $t = (51, 52, 53, 54)$, the signal takes on values $y = (5, 9, 7, 10)$. The 4-tuple created by these points would be $(4, 2, 3, 1)$, indicating the largest amplitude occurs in the 4th time point, followed by the 2nd time point, and so on. In a time series with N points, there is a total of $(N - d + 1)$ d-tuples: $(x_1, x_2, ..., x_{N-d+1})$. For each embedding dimension d, there are $d!$ possible permutations, which is the number of possible amplitude ordering combinations. From the d-tuples, one could compute the relative frequency or the probability for a given amplitude ordering permutation type π:[8]

$$p(\pi) = \frac{\#\{t | t \leq N - d + 1, (x_t) \text{ has type } \pi\}}{N - d + 1} \tag{4}$$

The BP probability space thus has dimension of $d!$, and is normalized to 1. The way the BP probability distributions are presented is that one ranks the relative frequencies of each permutation from the highest to lowest and plot the relative frequencies against bin number (permutation number of the amplitude ordering) using a semi-log scale. If the relative frequency of a permutation is zero, that bin is empty on presented BP probability plots. In this way, the BP probability distribution is capable of detecting the preferable population in the temporal signal and thus the structure of amplitude orderings.

The choice of d depends on the value of N and the time scale $d\Delta t$ of the structure being investigated, where Δt is the time interval between adjacent data points.[13] On one hand, one should choose a small d such that $N/d! \gg 1$ to obtain a reliable result. On the other hand, d cannot be so small that relevant structures in the signal (e.g. Lorentzian pulses) cannot be represented appropriately. A typical choice of d is usually within the range of $3 \leq d \leq 7$. In this work, $N = 20,000$ and $d = 6$ were used for all the BP probability and

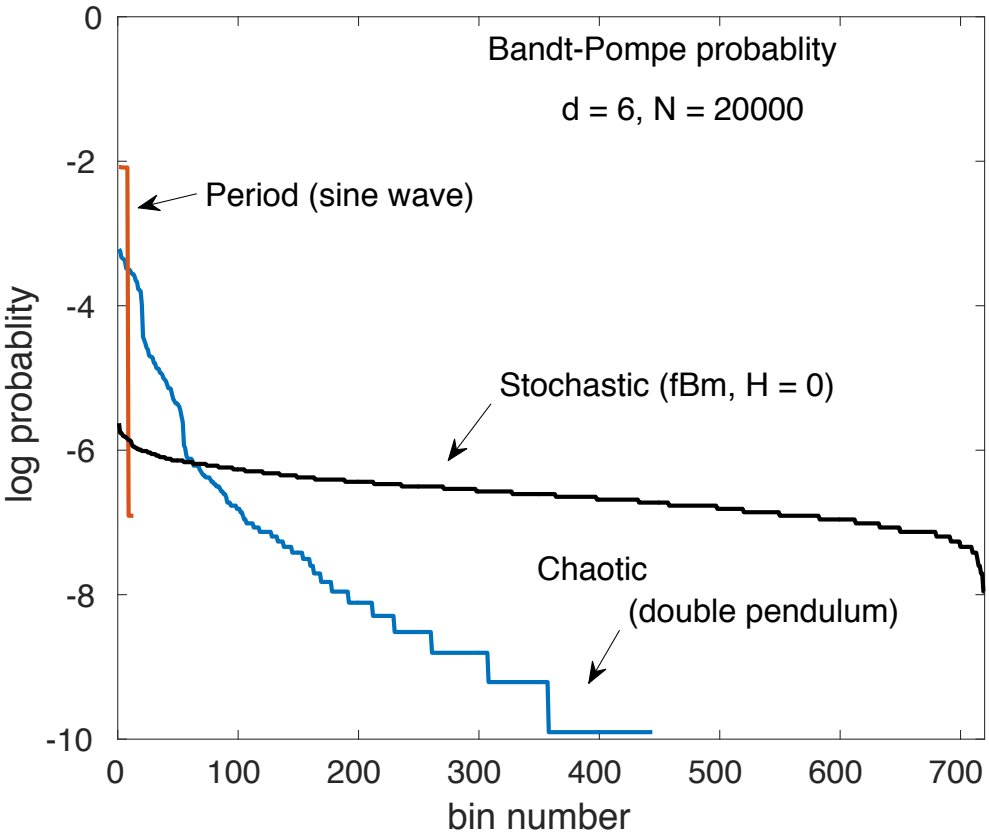

FIG. 1. The BP probability distributions of stochastic, chaotic, and periodic test data with $N = 20,000$ and embedding dimension $d = 6$. The stochastic signal is the fractional Brownian motion with Hurst exponent $H_{\text{exp}} = 0$,[28] and it is uniformly distributed over the BP probability space. The chaotic signal is the trajectory of a ball in a double pendulum system[29], and it has a range of highly-occupied states and a range of unoccupied states. The periodic test signal is a sine wave $f(t) = \sin(\omega t)$, where $\omega = (2\pi \cdot 500)$ rad/s, and it only has very narrow range of occupied states.

C-H plane analysis. With $N/d! \approx 27.3$, the number of d-tuples is large enough to capture the structure. With $d\Delta t = 1.2\mu$s, each d-tuple has a time scale that is comparable to the typical pulse width. Therefore, the resulting BP probability is able to capture relevant structures in the signal. Analyses using $d = 5$ and $d = 7$ were compared, but the qualitative results are the same. A more detailed study about how to choose can be found in the Ph.D thesis of B. Frettman.[30]

In general, a stochastic signal has a relatively uniform BP distribution because it does not have a preferable amplitude ordering and thus occupies all the BP probability space equally likely. A chaotic signal would have a peak around small bin number because it contains structures and thus has preferable states in the BP probability space: the distribution has a range of states with high relative frequencies along with a wide range of unoccupied or low-occupied states. A periodic signal has repeating structures and thus has very few occupied states and is very sharply peaked in the probability space. In Fig. 1, BP distributions generated from three groups of test signals (stochastic, chaotic, and periodic) are shown.

The shape of BP probability distributions provides a qualitative view of the nature of a given time history, and it can be quantified using the complexity-entropy plane (C-H plane). This technique was introduced by Rosso, *et al*[9] to distinguish chaotic signals from noise. The C-H plane consists of two statistical measurements: the normalized Shannon

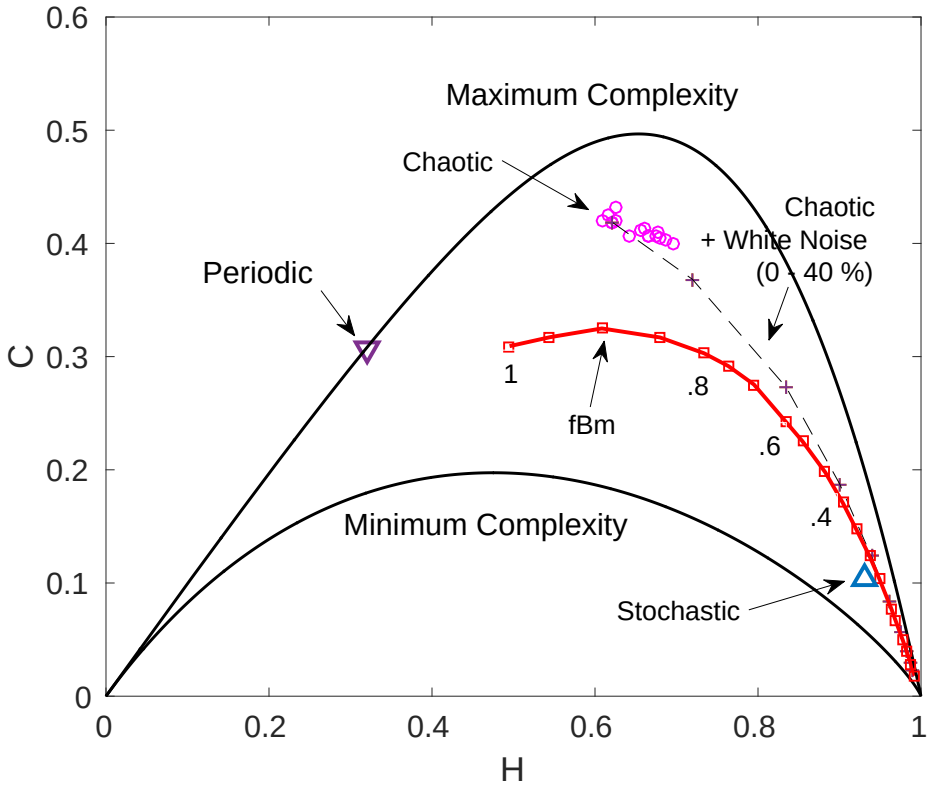

FIG. 2. Periodic, chaotic, and stochastic signals fall on different parts of the C-H plane. The red curve shows fractional Brownian motions with different Hurst exponents (marked below the red curve) $0 \leq H_{\text{exp}} \leq 1$,[28] which is purely stochastic. The second set of stochastic data is generated using randomly distributed Lorentzian pulses with different pulse widths (marked with blue triangle), which will be discussed later in section V. The periodic test signal is a sine wave $f(t) = \sin(\omega t)$, where $\omega = (2\pi \cdot 500)$ rad/s; it has relatively low C and H. The chaotic data was generated using the trajectories in a double pendulum system with different initial conditions;[29] the points are located in between the maximum complexity curve and the fractional Brownian motion curve. The dashed trajectory was corresponds to adding 0 - 40% white noise to one of the chaotic time traces. H increases as the percentage of white noise increases.

entropy H and the Jensen-Shannon complexity C. The Shannon entropy measures the disorder or the uncertainty of a physical process described by a probability distribution. For example, for a given probability distribution, if the outcome of a physical process is random or unpredictable, the process has high entropy. Statistical complexity measures the structure of a time signal in terms of the uncertainty of a system and its "distance" from complete disequilibrium.[31]

First, the Shannon entropy S for a given probability distribution $P = (p_1, p_2, ..., p_{d!})$ with d! possible states is defined as:

$$S(P) = -\sum_{i=1}^{d!} p_i \log_2 p_i \tag{5}$$

The normalized Shannon entropy H is then computed by dividing S by the maximum entropy, which corresponds to uniform probability distribution P_e, with $p_i = 1/d! \; \forall \; i \in [1, d!]$. $S_{\text{max}} = \log_2 d!$. The uniform distribution corresponds to the most random/unpredictable system, and thus has maximal entropy.

$$H(P) = \frac{S(P)}{S_{\max}} = -\frac{1}{\log_2 d!} \sum_{i=1}^{d!} p_i \log_2 p_i \tag{6}$$

where $0 \leq H(P) \leq 1$.

The statistical complexity of a given probability distribution P is defined as the product of entropy and disequilibrium, the "distance" between P and P_e.[31] There are different definitions of complexity depending on how disequilibrium is defined. In *Rosso, et al*,[9] the disequilibrium $Q_J(P)$ is defined in terms of the Jensen-Shannon divergence D_{JS}, given as:

$$Q_J(P) = Q_0 \cdot D_{JS} = Q_0 \left[S(\frac{P+P_e}{2}) - \frac{S(P)}{2} - \frac{S(Pe)}{2} \right] \tag{7}$$

where the notation $\frac{P+P_e}{2}$ denotes adding the BP probability p_i to the uniform probability $p_e = 1/d!$ and then dividing by 2 $\forall\ i \in [1, d!]$. Q_0 is a normalized constant $Q_0 = -2\left[\frac{d!+1}{d!}\log_2(d!+1) - 2\log_2(2d!) + \log_2 d!\right]^{-1}$ such that $0 \leq Q_J(P) \leq 1$.

The complexity of a BP probability P is then defined as,

$$C(P) = Q_J(P) \cdot H(P) \tag{8}$$

$$C(P) = -2\frac{S(\frac{P+P_e}{2}) - \frac{S(P)}{2} - \frac{S(Pe)}{2}}{\frac{d!+1}{d!}\log_2(d!+1) - 2\log_2(2d!) + \log_2 d!} H(P) \tag{9}$$

For each given BP probability distribution, there is a corresponding C and H value and thus a point on the C-H plane. Since BP probabilities with the same entropy do not necessarily have the same complexity, the C and H can be used as independent parameters for the investigated signals when plotting the C-H plane.[13] For a given H, there is a maximum and a minimum possible complexity values, giving a complexity boundary for $0 \leq H \leq 1$. All points should fall between the two curves. *Calbet, et al*[32] and *Martin, et al*[31] discussed the methods to solve for the extrema of different definitions of complexity using Lagrangian multipliers in detail. For the Jensen-Shannon complexity, the probability distributions that minimize and maximize the complexity are given in Table I and Table II respectively. The boundaries are different for different choice of d.

TABLE I. The probability distributions that minimize the complexity.

Number of states with f_j	f_j	Range of f_j
1	$f_{\min}$	$[\frac{1}{d!}, 1]$
$d! - 1$	$\frac{1 - f_{\min}}{1 - d!}$	$[0, \frac{1}{d!}]$

Different locations on the C-H plane correspond to different types of processes generating the corresponding temporal signals. Figure 2 shows what different regions on the C-H plane represent: complexities and entropies of double pendulum trajectories (chaotic),[29] chaotic signals with different percentages of added white noise (transitioning from dominantly chaotic to dominantly stochastic),[33] and a sine wave (periodic). Generally speaking, periodic systems have low entropies and complexities because of their repetitive patterns and predictability. Chaotic systems have high complexities and medium-ranged entropies.

TABLE II. The probability distributions that maximize the complexity, where $n \in \mathbb{Z}$ and $0 \leq n \leq (d! - 1)$; the maximum complexity curve is not smooth

Number of states with f_j	f_j	Range of f_j
n	0	0
1	$f_{\max}$	$\left[0, \frac{1}{d!-n}\right]$
$d! - n - 1$	$\frac{1 - f_{\max}}{d! - n - 1}$	$\left[\frac{1}{d! - n - 1}, \frac{1}{d! - n - 1}\right]$

Stochastic systems have high entropies and low complexities because they are highly uncertain and they are close to the uniform distribution. While there is no hard boundary between chaotic and stochastic signals, the fractional Brownian motion (fBm)[28] is a useful curve to compare the data points with: the closer a point is to the fBm line from above, the more stochastic it is. Points on the fBm line or below are considered purely stochastic.

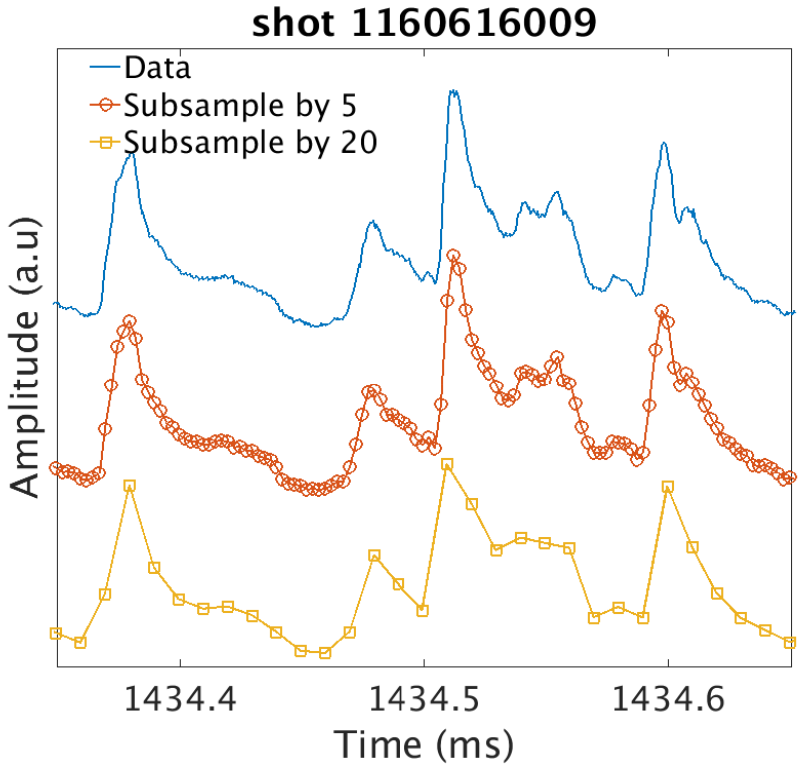

FIG. 3. Turbulent fluctuations obtained by the gas puff imaging (GPI) with different subsampling rate r_s show the effect of subsampling on temporal signals. The first signal (blue) is with $r_s = 1$ (no subsampling); high frequency noise is observed. The second signal (red) is with $r_s = 5$. At this subsampling rate, the original structure of the signal is retained while getting rid of the high frequency noise. The third signal (yellow) shows $r_s = 20$. This sampling rate fails to capture the true nature of this signal.

C. Subsampling

Subsampling is a technique being applied to the C-H analysis on signals with high frequency noise.[14] Although subsampling is not necessary for refletometry analysis, it is re-

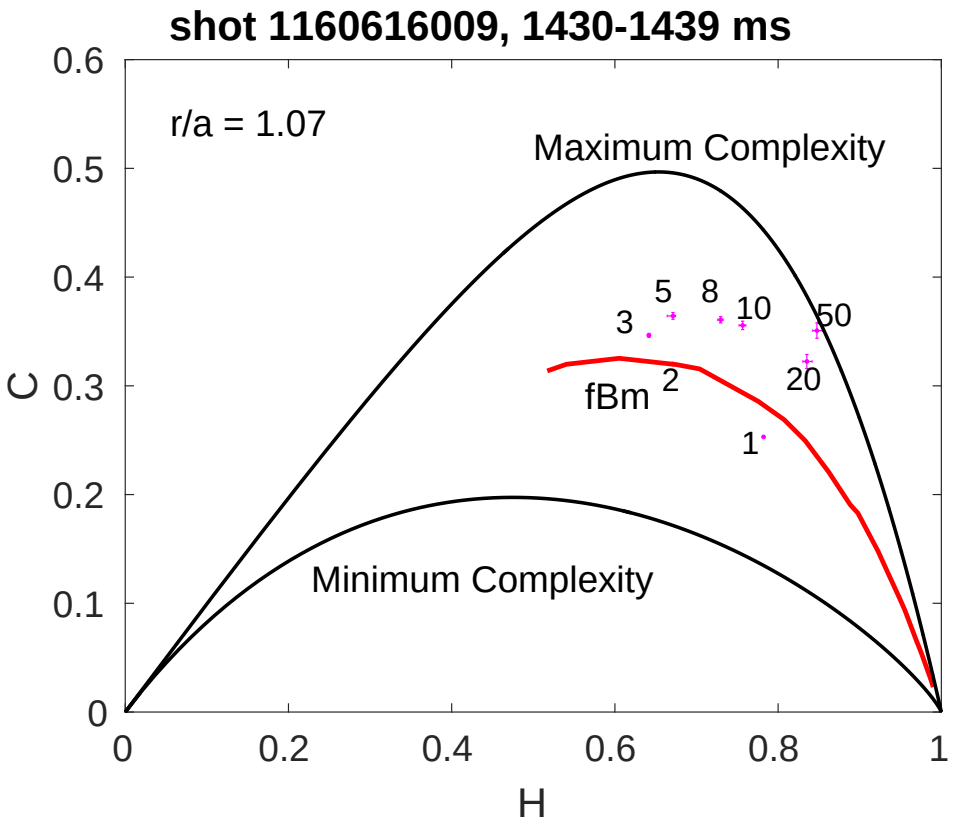

FIG. 4. The GPI data with different subsampling rate r_s's on the C-H plane shows that $r_s = 5$ is the best subsampling rate to apply. With $r_s = 1$, the data point is below the fBm line. As r_s increases to $r_s = 5$, points move towards the chaotic region. As r_s keeps increasing, points move back towards the stochastic region, meaning the signal is over-subsampled. Notice that when $r_s = 50$, the point falls close to the C_{max} curve; this is because when the sampling rate is too big, N/r_s is small such that there are only a few occupied states in the BP probability distributions, which assemble the distributions that maximize the complexity.

quired for the GPI analysis because the signal is dominated by white noise above 300 kHz (see fig. 11 for example).

When calculating the BP probability, if $d\Delta t$ is small compared to the time scales of interest (e.g. structures in the signal), each d-tuple is strongly influenced by the high frequency noise rather than the actual structure of the signal being investigated. Therefore, subsampling is required to ensure that the set of d-tuples reflects the actual structure in the data. To compute the BP probability, one should choose a set of N equally-spaced points. To perform subsampling on the dataset is to increase the spacing between adjacent time points by a factor of the subsampling rate, denoted as r_s, which is essentially to decrease the Nyquist frequency by a factor of r_s. In this way, r_s sets of data points with size N/r_s are obtained, which correspond to a number of r_s different BP probability distributions and points on the C-H plane (fig. 4). Errorbars can be obtained by calculating the standard deviation of the set of Cs and Hs corresponding to a given dataset. The choice of r_s is not arbitrary but rather restricted. It is important to choose a best r_s that is not only able to remove the noise component but also able to resolve the actual nature of the signal (fig. 3). Another problem with a large r_s is that $N/(r_s \cdot d!)$ might be too small such that the BP probability distribution is not reliable even if the structure in the temporal signals could be captured.

IV. EXPERIMENTAL SIGNAL ANALYSIS

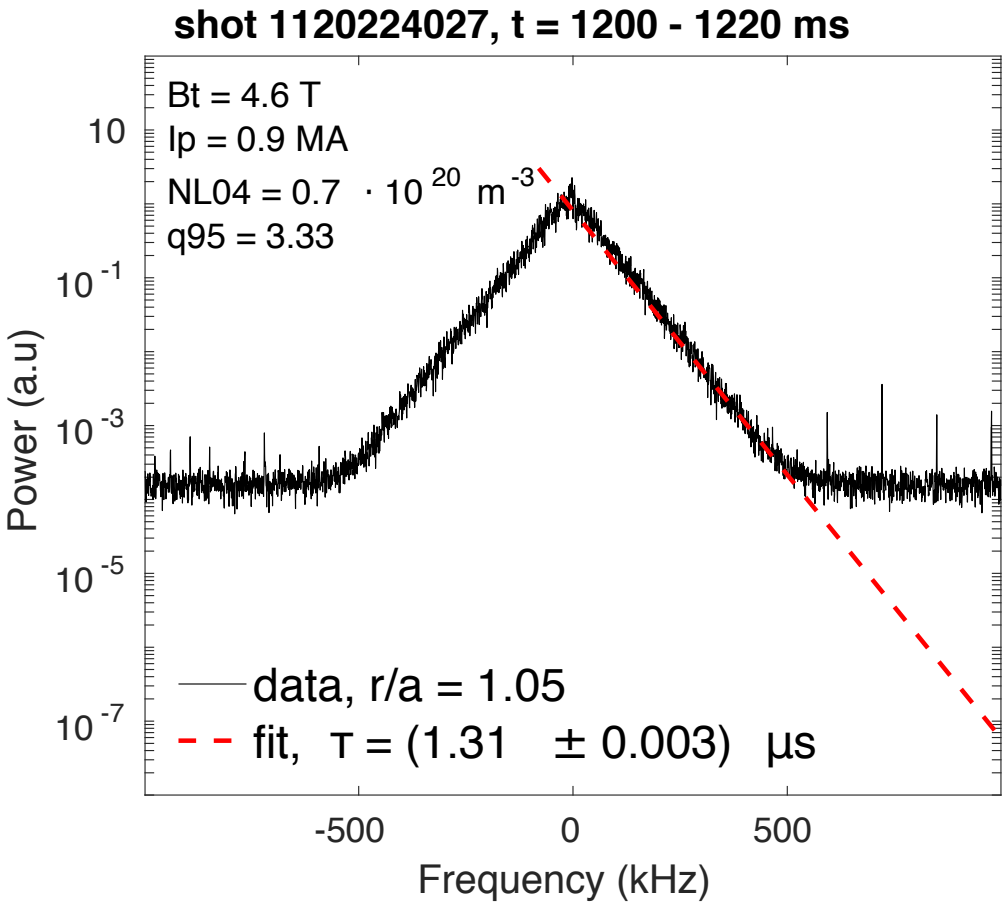

FIG. 5. A typical power spectrum of edge density fluctuations from L-mode plasmas as measured by reflectometry exhibits clear exponential shape; fitting the spectra to $P(\omega) \propto \exp(-2\omega\tau)$ gives the pulse width τ. The power spectra are normalized.

This section utilizes the three techniques introduced in the previous section to address the question of whether the turbulent fluctuations in the Alcator C-Mod tokamak are generated by chaotic or stochastic processes. As noted previously, the edge fluctuations being analyzed are those from the O-mode reflectometry and the GPI. L-mode plasmas were analyzed in detail and a brief overview of H-mode and I-mode signals is also included. In all cases: (1) the edge power spectra exhibit a clear exponential shape $P(\omega) \propto \exp(-2\omega\tau)$; (2) the BP probability distributions show a range a concentration of probability in a subset of permutations; and (3) the generated points on the C-H plane fall on the chaotic regions. These three observations are a strong indication that the process generating edge density fluctuations in Alcator C-Mod is chaotic in nature.

A. Exponential power spectra

As mentioned earlier, reflectometer data from each channel is complex, consisting of a inphase (real) part and a quadrature (imaginary) part. Therefore, the power spectra presented have both positive and negative frequencies that are not necessarily symmetric

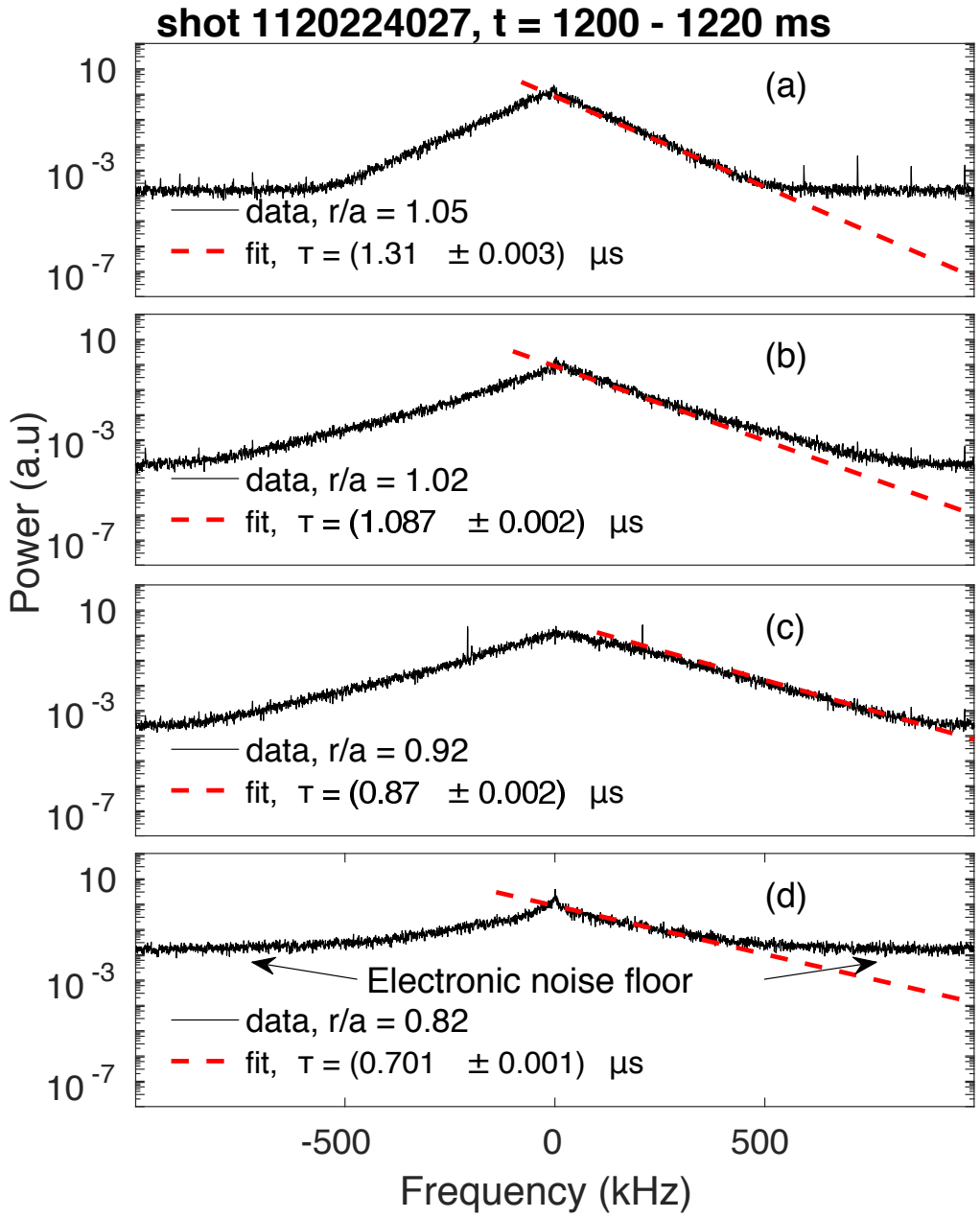

FIG. 6. Normalized power spectra from four different reflectometer channels (different major radii in the machine) shows a trend that τ decreases as the major radii decreases.

around the zero frequency. Figure 5 shows power spectra for reflectometer signals inside and outside of the last closed flux surface. These power spectra were fitted to the following equation:

$$\tilde{P}(f) = A \cdot e^{-4\pi\tau f} + \text{const.} \tag{10}$$

where τ is the pulse width of the corresponding Lorentzian pulses in time.

To obtain the best fit and the error, a technique called maximum likelihood estimation (MLE) was used.[34] It is a technique to optimize the parameter that fits data to a model by

maximizing the likelihood function of the model. The error can be obtained by calculating the standard deviation or the square root of the variance. For an exponential fit, we use the following normalized model and treat it as a probability distribution:

$$p(f) = A \cdot e^{-bf} = b \cdot e^{-b(f-f_{\min})} \tag{11}$$

where $b = 4\pi\tau$, $f \geq f_{\min}$ and $f_{\min} > 0$ for $p(f)$ to be normalizable.

Given a frequency-dependent power spectrum P, we use it as a probability distribution with frequency dependence, and generate a set of n values of $\mathbf{f} = \{f_i\}$ based on the distribution. The probability that the data is generated from this distribution is proportional to the log-likelihood of the dataset $\mathbb{L}$, defined as follows,

$$\mathbb{L} = \ln P(\mathbf{f}|b) = n \ln b + nbf_{\min} - b\sum_{i=1}^{b} f_i \tag{12}$$

Maximizing $\mathbb{L}$ by taking the derivative of $\mathbb{L}$ with respect to b, setting it to zero and then solving for b:

$$b = \frac{1}{\frac{1}{n}(\sum_{i=1}^{n} f_i) - f_{\min}} \tag{13}$$

The error of the optimal parameter can be obtained by first taking the exponential of the log-likelihood function (which is the likelihood function) and then calculating the half width of the maximum likelihood function, i.e: the standard deviation σ_b,

$$\exp(\mathbb{L}) = b^n \exp\left[b\left(nf_{\min} - \sum_{i=1}^{n} f_i\right)\right] \tag{14}$$

Define $a = nf_{\min} - \sum_{i=1}^{n} f_i$.

$$< b^2 >= \frac{\int_0^\infty b^{n+2} e^{ab}}{\int_0^\infty b^n e^{ab}} = \frac{(n+1)(n+2)}{a^2} \tag{15}$$

$$< b >= \frac{\int_0^\infty b^{n+1} e^{ab}}{\int_0^\infty b^n e^{ab}} = \frac{n+1}{a} \tag{16}$$

$$\sigma_b = \sqrt{< b^2 > - < b >^2} = \frac{\sqrt{n+1}}{\sum_{i=1}^{n} f_i - nf_{\min}} \tag{17}$$

which gives the error of the slope. The uncertainty on the evaluation of τ, $\sigma_\tau = -\sigma_b/4\pi$.

Historically, power spectra of turbulent fluctuations have been presented in log-log scale because the Kolmogorov 5/3 law of turbulence[35] states that the turbulent power spectra should fit to power laws. A quantitative assessment on whether a power law model or an exponential model provides a better fit to the edge turbulence data is Akaike information criterion (AIC).[34,36] The AIC is a measure of the relative quality of statistical models for a given set of data. For a given dataset $\mathbf{f_i}$, the corresponding AIC is defined as,

$$\mathrm{AIC}_i = -2 \ln \mathbb{L}_i(\hat{\theta}_i|\mathbf{f}) + 2K_i \tag{18}$$

where $\mathbb{L}_i$ is the log-likelihood function for a given model. $\hat{\theta}_i$ is the most probable parameter; K_i is some constant, and is the same for power law and exponential models.

The Akaike weights are the relative likelihood of each model (normalized to 1):

$$w_i = \frac{e^{-\Delta_i/2}}{e^{-\Delta_1/2} + e^{-\Delta_2/2}} \tag{19}$$

where $\Delta_i = \mathrm{AIC}_i - \mathrm{AIC}_{\min}$.

For the sake of completeness, the log-likelihood of a normalized power law model $p(f) = \frac{\alpha-1}{f_{\min}} \cdot \left(\frac{f}{f_{\min}}\right)^{-\alpha}$ is given as follows,

$$\mathbb{L} = \ln P(\mathbf{f}|\alpha) = \sum_{i=1}^{n} \left[\ln(\alpha - 1) - \ln f_{\min} - \alpha \ln \frac{f_i}{f_{\min}}\right] \tag{20}$$

In all presented cases, the Akaike weight of the exponential model is 1 and that of the power law model is 0, which quantitatively confirms that the exponential model is a better fit than the power law fit.

Power spectra at different major radii are shown in Fig. 6. Different reflectometer channels send out electromagnetic waves at different frequencies, and thus the cutoff layers are located at different major radii. The power spectra from all the first three channels exhibit clear exponential shapes. Figure 6 also shows a decreasing trend in τ as the major radii of the cutoff layer decreases. At the innermost radial location, $r/a = 0.82$, while the spectrum is approximately consistent with an exponential, the low signal-to-noise ratio makes it harder to determine the shape.

B. Lorentzian pulses

Pulses with an approximately Lorentzian shape are found in the time signals from the reflectometer, consistent with the observation of exponential power spectra[37]. A fitting routine was developed to locate and fit Lorentzian pulses in the time history. The routine takes a small time window of n points with length $n\Delta t$, $7 \leq n \leq 14$. It finds the extrema x_0 in the chosen window at time t_0, and fits the points in the time window to a Lorentzian function that passes through $(t_0,\ x_0)$.

$$L(t) = A\ \left[\frac{1}{\tau^2 - (t - t_0)^2} - \frac{1}{\tau^2}\right] + x_0 \tag{21}$$

where A is a normalization constant and τ is the pulse width of the pulse, defined to be half width at half maximum of the pulse.

If the fitted curve and the data agree within 5% on every point, the points in this time window are documented to be a pulse and then the routine moves to the next time window. When finding pulses, the routine choses to start with larger n such that the tails of a pulse is best captured while also avoiding counting pulses repeatedly.

The R^2, coefficient of determination, quantifies how well a curve fits to the data is calculated for fits to a Lorentzian function. For a given dataset $\{y_i\}$ and fit $\{f_i\}$, $R^2 = 1 - \frac{SS_{\mathrm{err}}}{SS_{\mathrm{tot}}}$, where $SS_{\mathrm{err}} = \sum (y_i - f_i)^2, SS_{\mathrm{tot}} = \sum (y_i - \bar{y})^2$.

Figure 7(a) shows a distribution of pulse widths found by the fitting routine. The average pulse width and pulse width found by fitting the power spectrum do not always agree. This disagreement could be explained by the overlap of pulses in the temporal signal (Fig. 7(b) and (c)). Simulations of overlapping pulses have indicated that overlapping pulses can cause the pulse widths determined by fitting the power spectrum to be greater than the actual value determined by fitting the time signal (Fig. 8). However, the value of τ found by

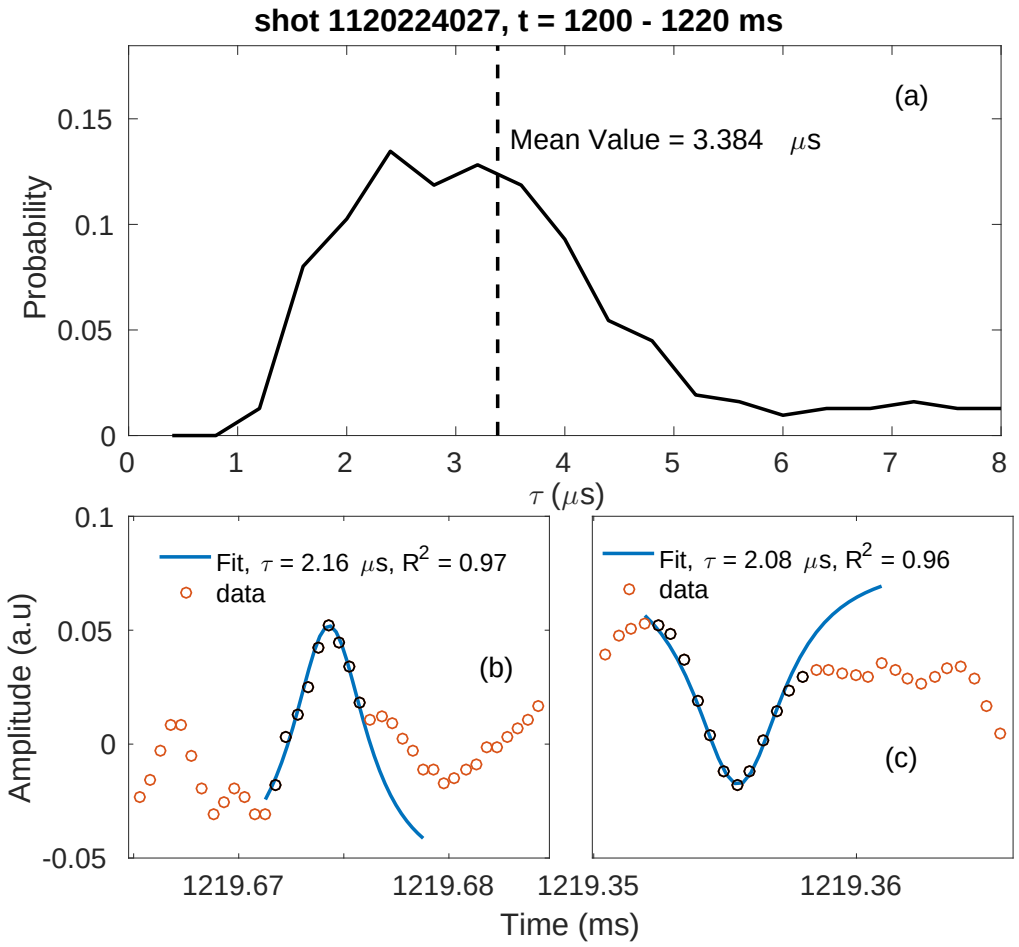

FIG. 7. (a) shows that the distribution of mean value of pulse widths found in the time history is larger than the τ calculated by fitting the power spectrum (fig. 5 and fig. 6). (b) and (c) are two typical Lorentzian pulses found by the automatic fitting routine; only the peak of pulses are visible due to superpositions. These data are from the reflectometer time series signals.

fitting the power spectra reflect the input pulse width(Fig. 8(a)). Therefore, fitting power spectra is a more sensitive method and it is used to find the pulse width for the rest of this work.

C. BP probability and C-H plane

Figure 9 shows the BP probability distributions of the inphase signal corresponding to the same shot in Fig. 6. The BP probability distribution for measurements at $r/a = 1.05, 1.02$ and 0.92 are qualitatively similar to the distribution for the double pendulum: there is a clear structure in the signal, with particular amplitude ordering permutations dominating the signal. At $r/a = 0.82$, the BP distribution looks more similar to noise (near uniform distribution across permutations); this is consistent with the low signal-to-noise at this location, so that the stochastic noise signal dominates the BP distribution. One additional BP distribution is shown in this figure for the case where the frequency of the reflectometer is too high to reflect within the plasma. This signal should primarily contain noise (electronic) and is consistent with fBm.

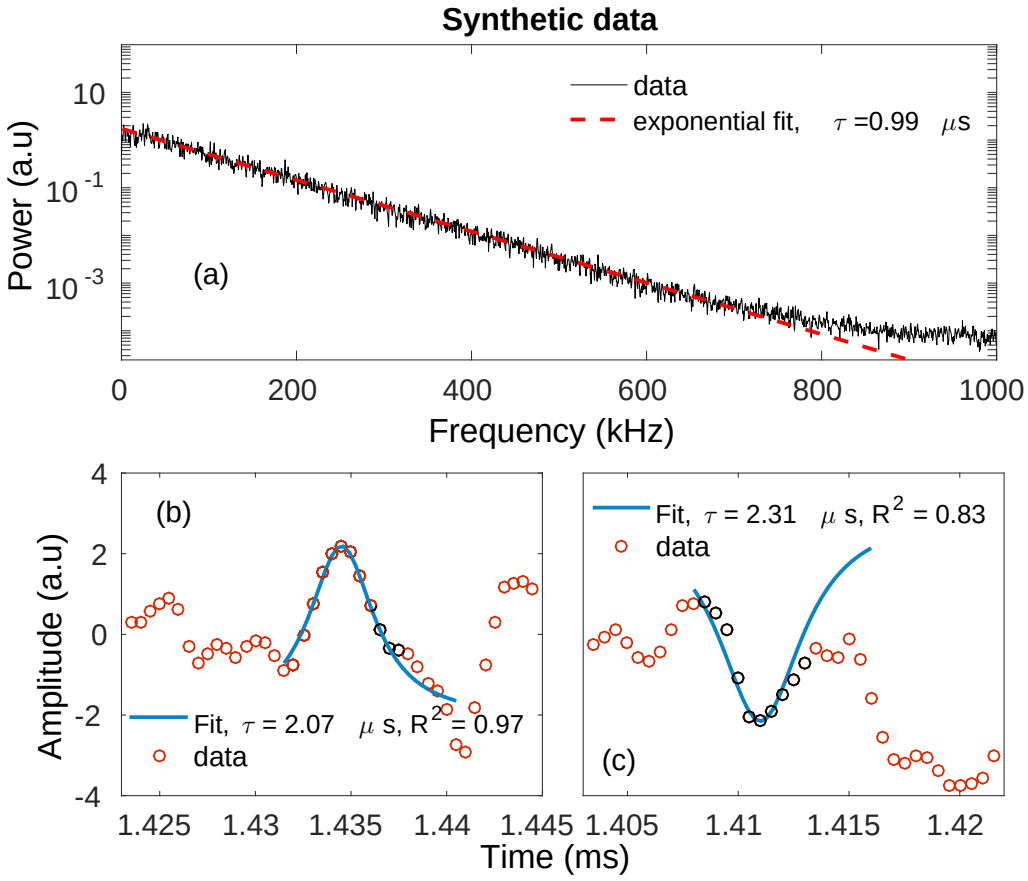

FIG. 8. Synthetic data of overlapping pulses with pulse width $1\mu s$. The pulse width calculated by fitting the power spectrum shows an agreement with the actual pulse width in (a). The pulse widths found by fitting time history using the automatic routine in (b) and (c) are about twice of the actual value due to superposition.

These BP probability distributions are used to place the time signals on the C-H plane, which is showin in Fig. 10. The fluctuations in the edge region ($r/a = 1.05, 1.02, 0.92$) are clearly in the chaotic region of the CH plane, with high complexity and moderate entropy. The data at $r/a \sim 0.86$ is located near the fBm line, which shows that the signals measured in the core are more stochastic. This is consistent with the low signal to noise at this location, where the dominance of electronic noise could explain the placement on the C-H plane.

D. Gas puff imaging (GPI) measurements

The same analyses (power spectra, BP probability, the C-H plane) were performed on the GPI data. Figure 11 compares a reflectometry inphase spectrum and a GPI spectrum at roughly the same radial position (r/a $\sim$ 0.99). Both spectra show an approximate linear shape on semi-log scales that is consistent with exponential power spectra. While reflectometry and GPI show the same result qualitatively, the GPI spectrum has a larger slope on this scale, which corresponds to a larger pulse width in time. The reason for this is presently unknown. Possible explanations include the fact that the exact cutoff layer of the reflectometry is unknown; the radial position measured by the reflectometer might be

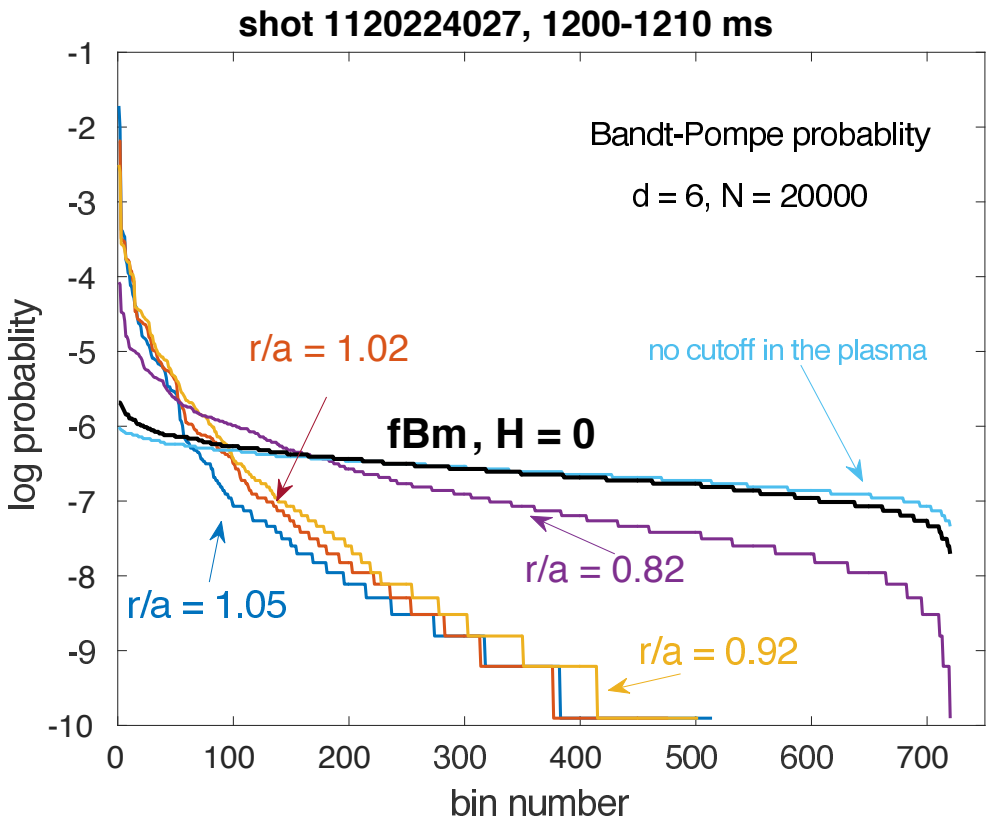

FIG. 9. The Bandt-Pompe probability distributions corresponding to the power spectra in figure 6 shows edge fluctuations have preferable states while core fluctuations do not.

slightly smaller than that from the GPI. Figure 6 shows that the spectra with smaller major radii have smaller pulse widths, which is a possible explanation of the discrepancy in slopes. Furthermore, as mentioned in previous sections, GPI-measured fluctuations depend on both density and temperature fluctuations and can be approximated as $\tilde{S}/\bar{S} \approx \alpha\tilde{n_e}/\bar{n}_e + \beta\tilde{T_e}/\bar{T}_e$, with $\alpha \sim 0.5$ and $\beta \sim 0.1$ under the conditions for this shot[38]. Depending on the amplitude of $\alpha\tilde{T_e}$ may or may not have a significant contribution to $\tilde{S}$. Therefore, the GPI was measuring a somewhat different quantity than the reflectometry.

Figure 12 shows the C-H plane locations of GPI fluctuation data at different major radii. GPI data at different radii require different subsampling rates as GPI has a higher noise floor than reflectometery (fig. 11). The subsampling rates chosen for the 7 radial positions are $[5, 5, 8, 3, 3, 3, 3]$ respectively. They were chosen based on the noise level and the C-H locations of different sampling rates. The C-H locations of different radii follow the same trend as reflectometry: the signals are more chaotic in the SOL and have a more dominant stochastic component closer to the core. Therefore, both power spectra and the C-H plane analysis from GPI data support the chaotic nature of the C-Mod edge density fluctuations.

E. Overview of H-mode and I-mode edge density fluctuations

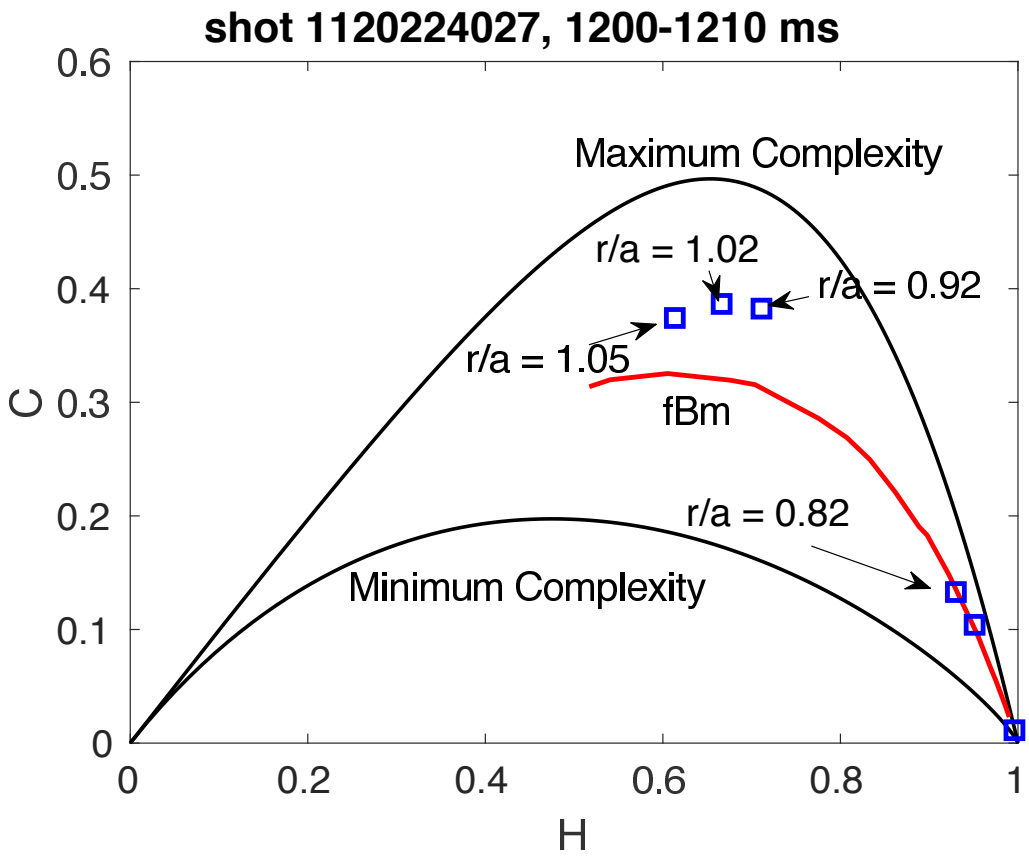

FIG. 10. The C-H plane locations corresponding to the BP probability distributions shown in figure 9 indicate that edge turbulence is strongly chaotic.

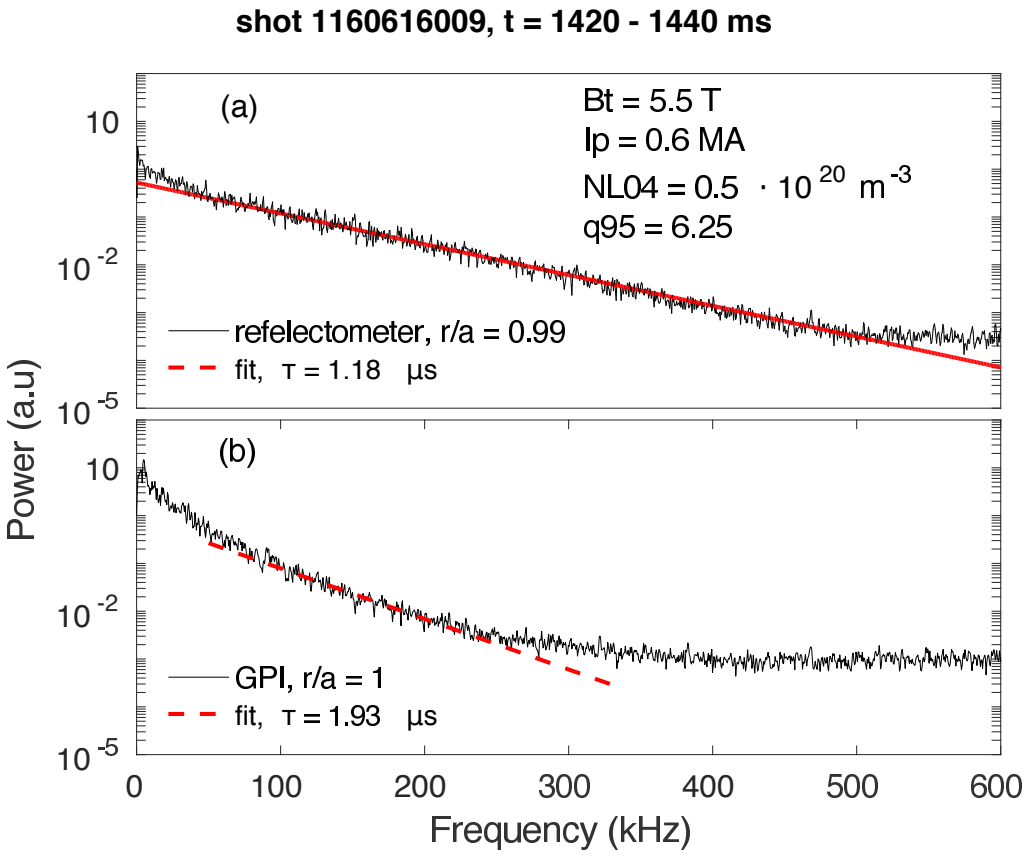

FIG. 11. A GPI spectrum is compared with the reflectometer spectrum from the same shot and same time interval. Both spectra have exponential shapes but they have different slopes.

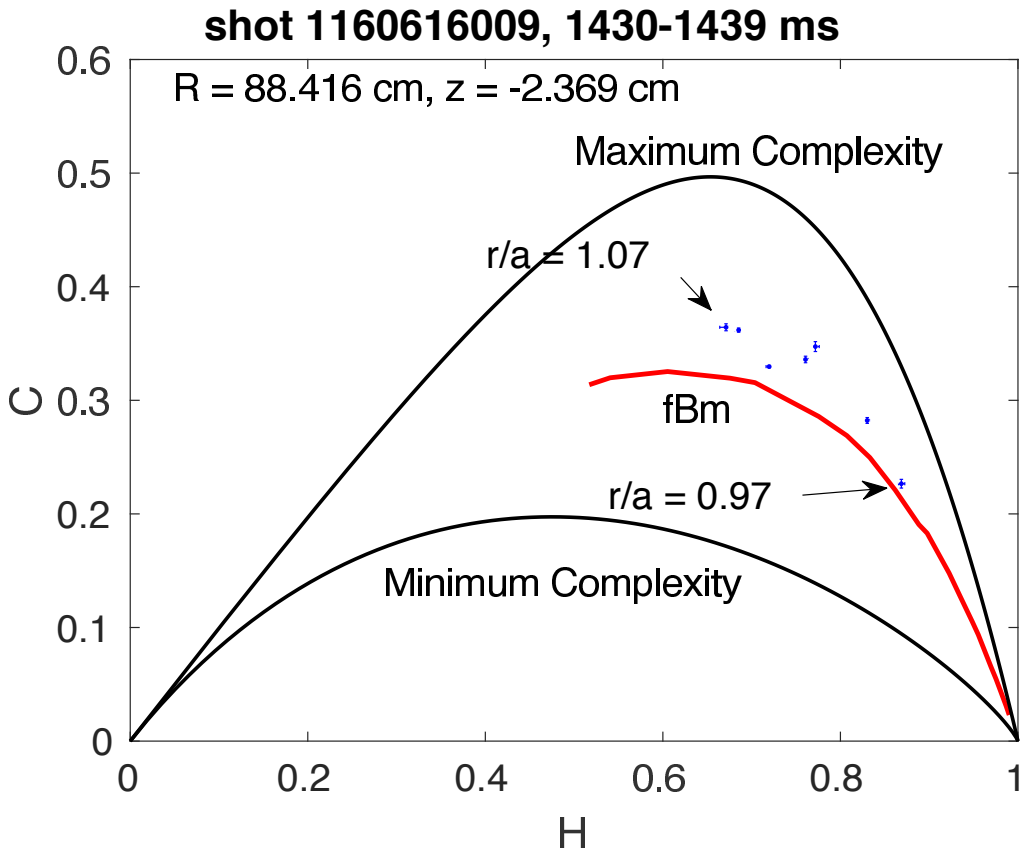

FIG. 12. The C-H plane locations of GPI show edge fluctuations are chaotic. Errorbars come from subsampling the signals.

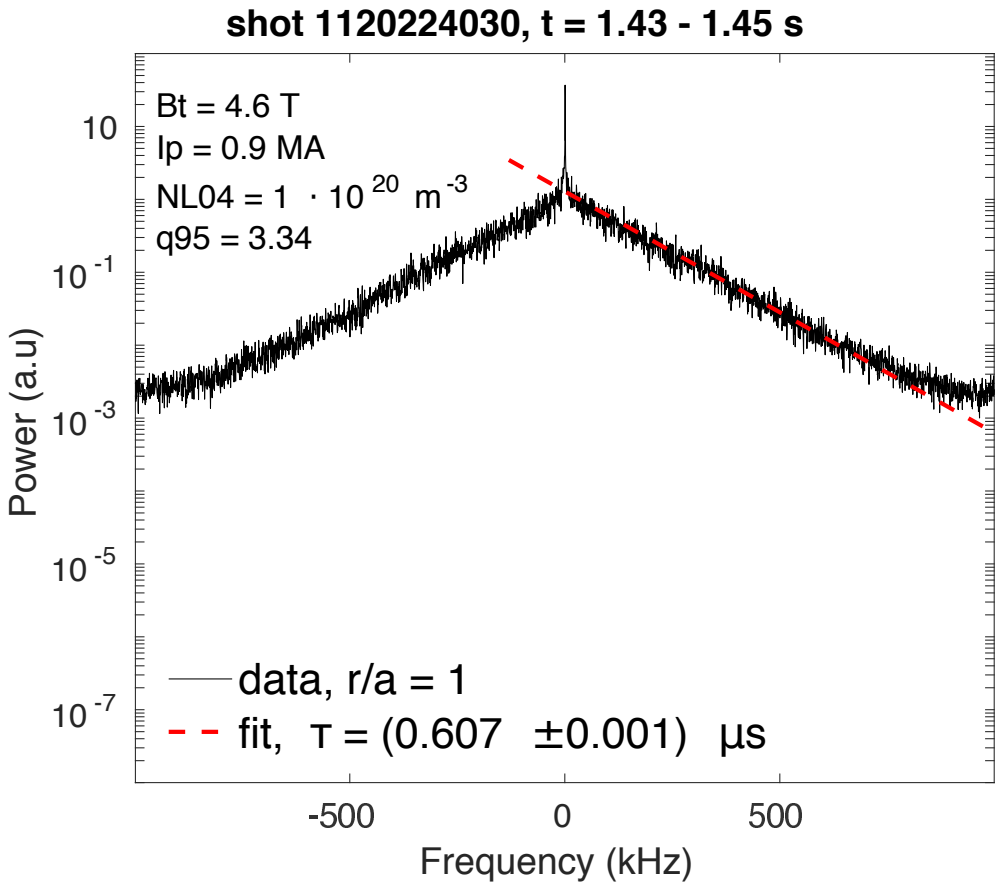

FIG. 13. A power spectrum of fluctuations measured with the reflectometer for an H-mode plasma near the SOL exhibit an exponential shape.

In addition to L-mode plasmas, H-mode and I-mode plasmas were studied. H-mode plasmas are characterized by sharp edge density and temperature gradients[39]. I-mode plasmas have an edge temperature gradient but their density profile is almost identical to L-mode; they have the same thermal-transport as H-mode but similar particle transport as in L-mode. [40]

Figure 13 shows a power spectrum of reflectometry-measured edge fluctuations measured during an H-mode plasma, which exhibit an exponential shape. Similar to L-mode plasmas, pulses were identified in the time signal in this case. Figure 14 shows the C-H plane locations corresponding to the power spectra in Fig. 13. The location on the C-H plane and trend with changing radius in this case is similar to what was observed in L-mode plasmas (see Fig. 10). The shape of the power spectrum and the C-H plane analysis indicate that H-mode edge fluctuations are generated by a chaotic process.

Figure 15 shows power spectra of reflectometry-measured edge fluctuations during an I-mode plasma, one just into the SOL ($r/a = 1.02$) and one just at the separatrix. The peak near 200 kHz in the spectrum measured at the separatrix is the weakly coherent mode (WCM), which is a typical feature of I-mode edge power spectra. The WCM is radially localized, and it does not appear in the SOL. Pulses are observed in the $r/a \sim 1$ time signal. However, the appearance of WCM makes it hard to determine if the remainder of the broadband spectrum is consistent with an exponential model. Therefore, the C-H analysis is necessary to identify the nature of the fluctuations with the presence of WCM. More extensive study of the WCM properties, such as interaction with the Geodesic Acoustic Mode (GAM), is beyond the scope of this work, but can be found in *Cziegler*[41]. The C-

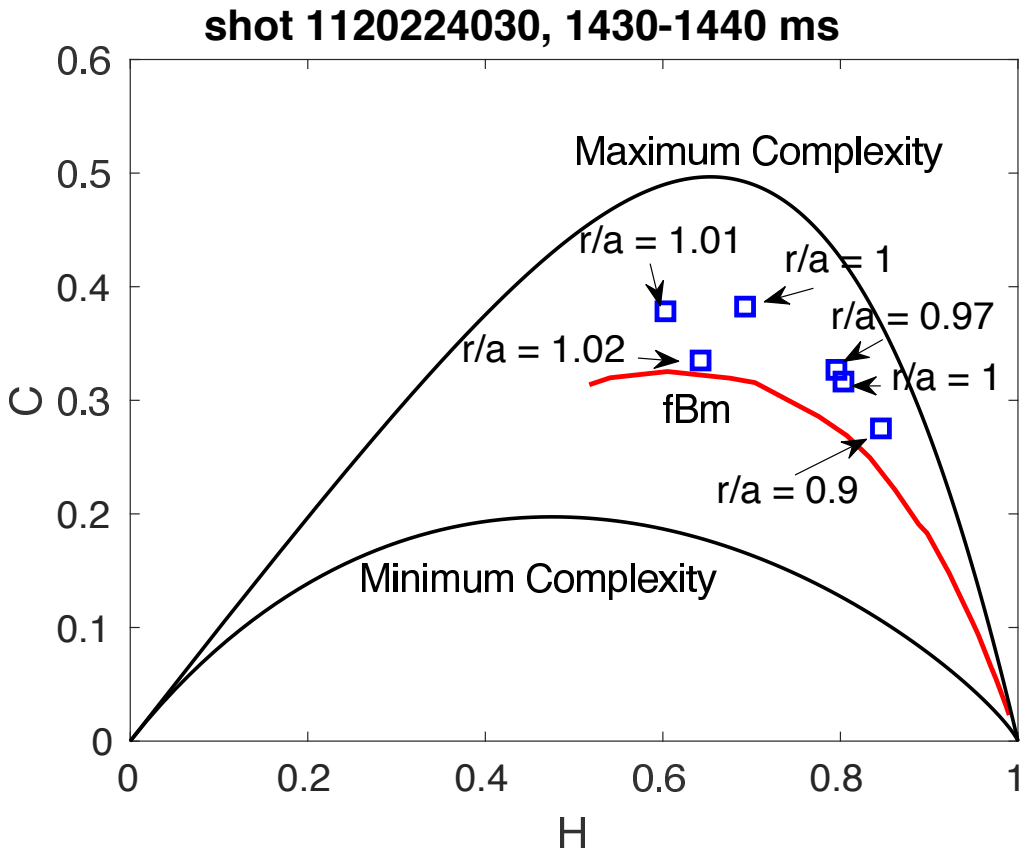

FIG. 14. The C-H plane locations corresponding to figure 13 (H-mode) indicate the chaotic nature of H-mode edge density fluctuations.

H plane locations of the I-mode plasma support the conclusion that edge fluctuations are produced by a chaotic process. Figure 16 shows a similar trend as the L-mode plasmas: the signals are strongly chaotic on the edge and have large noise component as measurements move toward the core.

V. DISCUSSION AND CONCLUSIONS

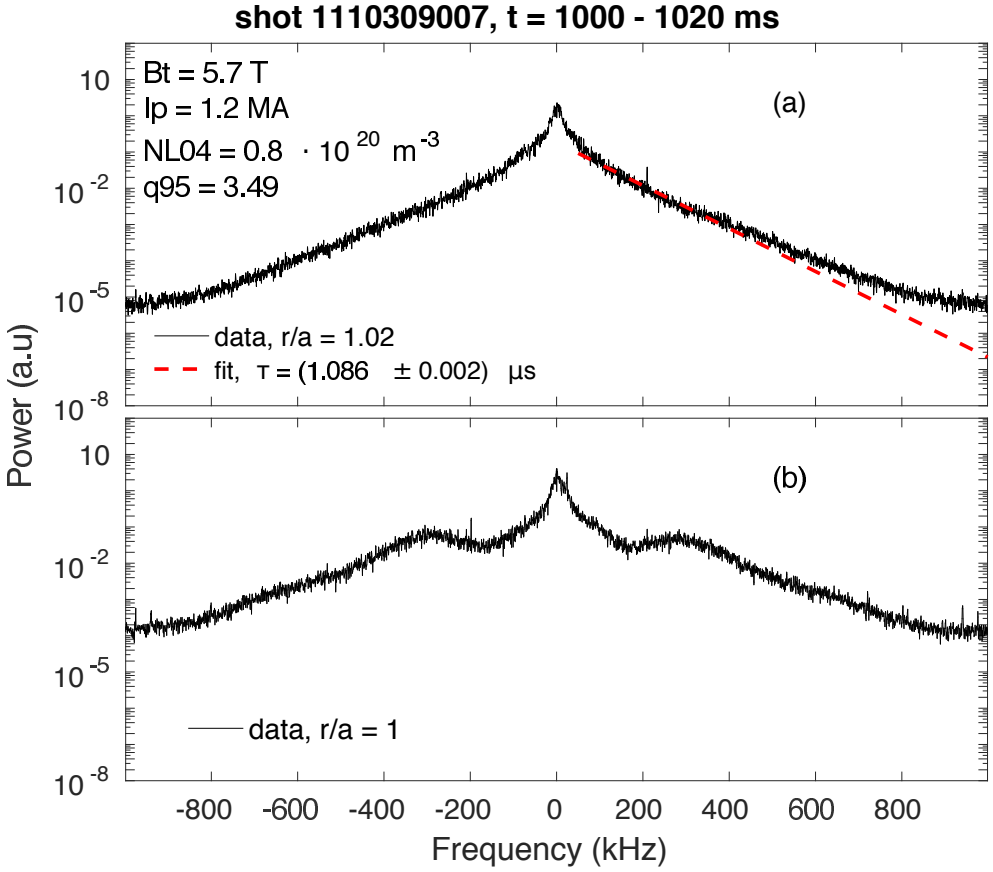

FIG. 15. Power spectra of reflectometry-measured fluctuations from an I-mode plasma (a) outside and (b) just inside SOL are compared. The spectrum outside the SOL exhibits exponential shape. The weakly coherent mode (WCM) appears around 200 kHz in the power spectra measured inside or at the SOL, making fitting the spectrum difficult.

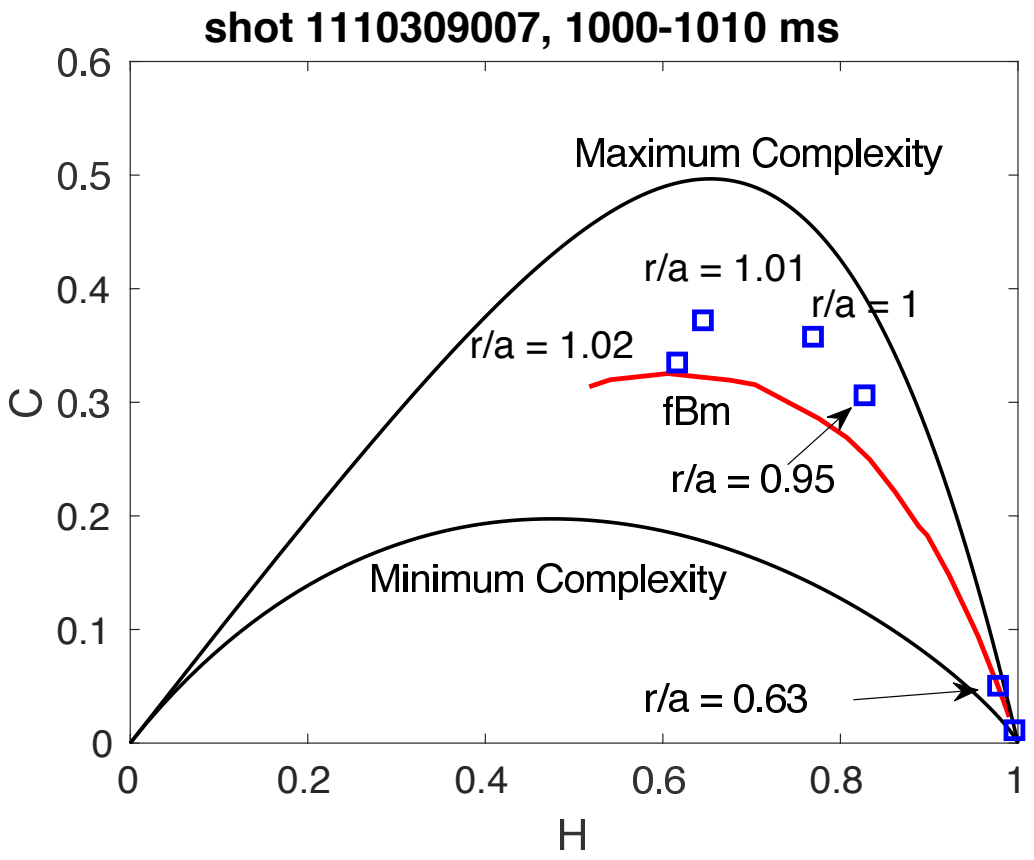

FIG. 16. The C-H plane locations corresponding to figure 15 (I-mode) indicate the chaotic nature of I-mode edge density fluctuations.

Edge density fluctuations measured in L-mode, H-mode and I-mode using reflectometry and GPI are found by these analyses to be chaotic. The reflectometry-measured signals have exponential power spectra and, consistent with the spectral shape, contain Lorentzian-shaped temporal pulses. Note that the GPI-measured spectra have a slight different shape, which might be due to the signals' dependence on temperature fluctuations. In addition, the complexity and entropy of the measured signals are computed and shown to fall on the chaotic region of the C-H plane. The exponential power spectra and the C-H locations together support the chaotic nature of the edge density fluctuations. The core turbulence is more stochastic on the C-H plane. However, with the small signal to noise ratio from the reflectometer in the core region, it is hard to establish the real nature of core turbulence, and new experiments will be required.

Similar experiments and analysis to those presented here were performed previously on many other toroidal and linear devices using different diagnostic techniques: the DIII-D tokamak[13] with the Doppler backscattering (DBS), the TJ-K stellerator,[16] and the Large Plasma Device (LAPD)[6,17] with Langmuir probes. In these experiments, Lorentzian-shaped pulses and exponential power spectra were identified and the chaotic nature of the edge density fluctuations was established. The normalized time scale associated with the exponential power spectra, $\tau f_{\rm ci}$, are within a factor of 2 in all these cases despite a wide range of plasma parameters.[13] For example, the typical magnetic field in the LAPD is 1000 G and that of the DIII-D tokamak is 3 T. The Langmuir probe data in the TJ-K yield the range of $\tau f_{\rm ci}$ between 3.7 and 5; experiments in the LAPD[6,17] reveal $\tau f_{\rm ci} = 6$ and in the DIII-D Doppler backscattering data, $\tau f_{\rm ci} = 8.6$ on average. However, the time scale in the Alcator C-Mod tokamak is drastically different than all of these other cases, with $\tau f_{\rm ci}$ around 30 - 50. Parameters of different devices are compared in table III, and it is not obvious which parameter controls the scaling of $\tau f_{\rm ci}$. A theoretical explanation of the large value of $\tau f_{\rm ci}$ compared to DIII-D[13] and LAPD and its relation to plasma transport models could be valuable to develop.

TABLE III. Comparison of parameters between different experiments; ν_e denotes the electron collision rate, $\nu_e = 1.33 \cdot 10^5 n_e T_e^{-3/2}$.

Device	$n_e(10^{20} \cdot \mathrm{m}^{-3})$	T_e (keV)	ν_e $(10^5 \cdot \mathrm{s}^{-1})$	τf_{ci}
C-Mod (L-mode)	0.35	0.1	14.7	40
C-Mod (H-mode)	1	0.3	8.1	27
DIII-D	0.26	2	0.12	8.6
LAPD	0.01	$5 \cdot 10^{-3}$	37	4
TJ-K	10^{-3}	$7 \cdot 10^{-3}$	2.3	3.7-5

The results from the Alcator C-Mod tokamak along with other toroidal and linear devices suggest that fluctuations in the edge region of magnetically-confined plasmas are generated via a chaotic process. Establishing the chaotic nature of edge turbulence in these devices provides a guide for further work the understand and perhaps control the processes that lead to turbulence and transport. In systems exhibiting low-dimensional chaos, as few as two interacting linear modes can explain the dynamics. Controlling one of these modes using, e.g. nonlinear three-wave interactions[42], may lead to the ability to control edge transport.

For future work, we note that this study did not establish the nature of the core density fluctuations. Although the analysis suggests that turbulence measured in the core region is chaotic, with large noise components, whether or not core turbulence is dominantly stochastic or chaotic in nature cannot be determined with the current set diagnostics considered here. Additional and new experiments on other tokamaks should be carried out. Exploring the chaotic nature of core turbulence could also be done theoretically, using, for example, nonlinear gyrokinetic simulations[43] to generate long-time series and then performing the same analysis as done here for experimental time series.

The diagnostics in this work could be improved. While reflectometry does not require time-averaging and does not perturb the plasmas, it has variation in its measured positions.

Several effects, including 2D effects and scattering, could also impact the interpretation of the results. GPI measures fluctuations at a relatively well-fixed position in space on a 2-D grid but had higher noise floor and might be influenced by temperature fluctuations, which makes direct comparisons between GPI and reflectometer difficult. Meanwhile, the injected neutral gas used for GPI could potentially perturb the plasma and complicate interpretation. Therefore, additional detailed modeling of the reflectometer and GPI diagnostics is required. Related to this, it could be very useful to generate either "toy-model" time series of the turbulence or use turbulence simulation time series outputs, and apply "synthetic diagnostics" that mimic the reflectometer and GPI[44] signals and look for evidence of chaotic dynamics in these synthetic time series. It would also be beneficial to use a third diagnostic, such as the mirror Langmuir probe at C-Mod,[45] to compare with reflectometry and GPI data.

Some studies of C-Mod GPI data, as well as Langmuir probe data from K-STAR and TCV indicate stochasticity in edge fluctuations.[46–50] Recent modeling work has shown that a random distribution of pulse widths can result in power law spectra, even if the model time series is composed of only Lorentzian pulses.[51] However, previous works[46–50] did not include the C-H plane analysis, and we have demonstrated that applying the C-H analysis to a set of synthetic data with Lorentzian pulses with randomly distributed pulse widths will indeed show its stochastic nature (the blue triangle in fig. 2). Therefore, the C-H plane analysis is capable of distinguishing the chaos and stochasticity of this type of synthetic data, and a chaotic description is valid for the data presented in this study. This suggests that future studies should include C-H plane analysis as a technique to show the nature of turbulence fluctuation data.

While the C-H plane analysis can be used as evidence to support the conclusion that the fluctuations are chaotic, it has to be combined with other methods such as power spectra analysis, because there is no definite boundary between chaotic and stochastic signals. It is also difficult to compare the C-H locations of different reflectometer channels because there is no parameter that accesses the "degree of chaos" of a signal. Therefore, developing such a parameter to quantify the "degree of chaos" can be beneficial for understanding the turbulent nature. Using the power spectrum as a part of a test for chaotic dynamics though also involves some uncertainty. For example, real diagnostic data often do not always have a wide enough dynamic range (e.g. a low noise floor) to capture enough orders of magnitude in the measured spectrum to faithfully capture the shape. Therefore, all three techniques, power spectra, the BP probability distribution, and the C-H plane, have to be combined to identify the nature of turbulent fluctuations, and it would be valuable to apply these techniques to analyze the data in other devices with various diagnostics.

ACKNOWLEDGMENTS

Discussions with G. Morales, J. Maggs, J. Bonde, M. Martin, and S. Dorfman are gratefully acknowledged. The authors thank V. Winters for her previous work. The experiments reported in the paper were performed in the MIT Plasma and Fusion Center. This work was supported by the U.S. Department of Energy Office of Science under Agreement DE-FC02-99ER54512 and DE-FC02-07ER54918-011.

REFERENCES

[1]J. E. Maggs and G. J. Morales, "Origin of Lorentzian pulses in deterministic chaos," Phys. Rev. E **86**, 015401 (2012).
[2]G. Staebler and J. Kinsey, "Electron collisions in the trapped gyro-Landau fluid transport model," Phys. Plasmas **17**, 122309 (2010).
[3]D. del Castillo-Negrete, B. Carreras, and V. Lynch, "Fractional diffusion in plasma turbulence," Phys. Plasmas **11**, 3854–3864 (2004).

[4]S. Zweben, J. Myra, W. Davis, D. D'Ippolito, T. Gray, S. Kaye, B. LeBlanc, R. Maqueda, D. Russell, D. Stotler, *et al.*, "Blob structure and motion in the edge and SOL of NSTX," Plasma Phys. and Control. Fusion **58**, 044007 (2016).
[5]J. Terry, S. Zweben, K. Hallatschek, B. LaBombard, R. Maqueda, B. Bai, C. Boswell, M. Greenwald, D. Kopon, W. Nevins, *et al.*, "Observations of the turbulence in the scrape-off-layer of Alcator C-Mod and comparisons with simulation," Phys. Plasmas **10**, 1739–1747 (2003).
[6]T. Carter, "Intermittent turbulence and turbulent structures in a linear magnetized plasma," Phys. Plasmas **13**, 010701 (2006).
[7]T. Rhodes, W. Peebles, E. Doyle, P. Pribyl, M. Gilmore, R. Moyer, and R. Lehmer, "Signal amplitude effects on reflectometer studies of density turbulence in tokamaks," Plasma Phys. and Control. Fusion **40**, 493 (1998).
[8]C. Bandt and B. Pompe, "Permutation entropy: a natural complexity measure for time series," Phys. Rev. Lett. **88**, 174102 (2002).
[9]O. Rosso, H. Larrondo, M. Martin, A. Plastino, and M. Fuentes, "Distinguishing noise from chaos," Phys. Rev. Lett. **99**, 154102 (2007).
[10]M. Zanin, "Forbidden patterns in financial time series," Chaos: An Interdisciplinary Journal of Nonlinear Science **18**, 013119 (2008).
[11]L. Zunino, M. Zanin, B. M. Tabak, D. G. Pérez, and O. A. Rosso, "Forbidden patterns, permutation entropy and stock market inefficiency," Physica A **388**, 2854–2864 (2009).
[12]G. Ouyang, X. Li, C. Dang, and D. A. Richards, "Deterministic dynamics of neural activity during absence seizures in rats," Phys. Rev. E **79**, 041146 (2009).
[13]J. Maggs, T. Rhodes, and G. Morales, "Chaotic density fluctuations in L-mode plasmas of the DIII-D tokamak," Plasma Phys. and Control. Fusion **57**, 045004 (2015).
[14]J. Maggs and G. Morales, "Permutation entropy analysis of temperature fluctuations from a basic electron heat transport experiment," Plasma Phys. and Control. Fusion **55**, 085015 (2013).
[15]P. J. Weck, D. A. Schaffner, M. R. Brown, and R. T. Wicks, "Permutation entropy and statistical complexity analysis of turbulence in laboratory plasmas and the solar wind," Phys. Rev. E **91**, 023101 (2015).
[16]G. Hornung, B. Nold, J. Maggs, G. Morales, M. Ramisch, and U. Stroth, "Observation of exponential spectra and Lorentzian pulses in the TJ-K stellarator," Phys. Plasmas **18**, 082303 (2011).
[17]D. Pace, M. Shi, J. Maggs, G. Morales, and T. Carter, "Exponential frequency spectrum in magnetized plasmas," Phys. Rev. Lett. **101**, 085001 (2008).
[18]J. Maggs and G. Morales, "Generality of deterministic chaos, exponential spectra, and lorentzian pulses in magnetically confined plasmas," Phys. Rev. Lett. **107**, 185003 (2011).
[19]E. Marmar, A. Bader, M. Bakhtiari, H. Barnard, W. Beck, I. Bespamyatnov, A. Binus, P. Bonoli, B. Bose, M. Bitter, *et al.*, "Overview of the alcator c-mod research program," Nuclear Fusion **49**, 104014 (2009).
[20]J. Hughes, D. Mossessian, A. Hubbard, E. Marmar, D. Johnson, and D. Simon, "-resolution edge Thomson scattering measurements on the Alcator C-Mod tokamak," Rev. Sci. Instrum. **72**, 1107–1110 (2001).
[21]A. Dominguez, *Study of density fluctuations and particle transport at the edge of I-mode plasmas*, Ph.D. thesis, Massachusetts Institute of Technology (2012).
[22]I. Cziegler, J. Terry, J. Hughes, and B. LaBombard, "Experimental studies of edge turbulence and confinement in Alcator C-Mod," Phys. Plasmas **17**, 056120 (2010).
[23]R. Maqueda, G. Wurden, D. Stotler, S. Zweben, B. LaBombard, J. Terry, J. Lowrance, V. Mastrocola, G. Renda, D. D' Ippolito, *et al.*, "Gas puff imaging of edge turbulence," Rev. Sci. Instrum. **74**, 2020–2026 (2003).
[24]L. Lao, H. S. John, R. Stambaugh, A. Kellman, and W. Pfeiffer, "Reconstruction of current profile parameters and plasma shapes in tokamaks," Nuclear fusion **25**, 1611 (1985).
[25]U. Frisch and R. Morf, "Intermittency in nonlinear dynamics and singularities at complex times," Phys. Rev. A **23**, 2673 (1981).
[26]H. Greenside, G. Ahlers, P. Hohenberg, and R. Walden, "A simple stochastic model for the onset of turbulence in rayleigh-bénard convection," Physica D **5**, 322–334 (1982).
[27]A. Libchaber, S. Fauve, and C. Laroche, "Two-parameter study of the routes to chaos," Physica D **7**, 73–84 (1983).
[28]B. B. Mandelbrot and J. W. Van Ness, "Fractional Brownian motions, fractional noises and applications," SIAM review **10**, 422–437 (1968).
[29]J. B. Marion and S. T. Thornton, *Classical dynamics of particles and systems* (Saunders, 1995).
[30]B. Friedman, *Simulation Analysis of Zero Mean Flow Edge Turbulence in LAPD*, Ph.D. thesis, University of California, Los Angeles (2013).
[31]M. Martin, A. Plastino, and O. Rosso, "Generalized statistical complexity measures: Geometrical and analytical properties," Physica A **369**, 439–462 (2006).
[32]X. Calbet and R. López-Ruiz, "Tendency towards maximum complexity in a nonequilibrium isolated system," Phys. Rev. E **63**, 066116 (2001).
[33]O. A. Rosso, L. C. Carpi, P. M. Saco, M. G. Ravetti, A. Plastino, and H. A. Larrondo, "Causality and the entropy–complexity plane: Robustness and missing ordinal patterns," Physica A **391**, 42–55 (2012).
[34]M. E. Newman, "Power laws, pareto distributions and zipf's law," Contemporary Phys. **46**, 323–351 (2005).
[35]A. N. Kolmogorov, "Dissipation of energy in locally isotropic turbulence," in *Dokl. Akad. Nauk SSSR*,

Vol. 32 (JSTOR, 1941) pp. 16–18.
[36] A. M. Edwards, R. A. Phillips, N. W. Watkins, M. P. Freeman, E. J. Murphy, V. Afanasyev, S. V. Buldyrev, M. G. da Luz, E. P. Raposo, H. E. Stanley, *et al.*, "Revisiting lévy flight search patterns of wandering albatrosses, bumblebees and deer," Nature **449**, 1044–1048 (2007).
[37] V. R. Winters, "Deterministic chaos in Alcator C-Mod edge turbulence," (2014), undergraduate thesis, Massachusetts Institute of Technology.
[38] I. Cziegler, *Turbulence and transport phenomena in edge and scrape-off-layer plasmas*, Ph.D. thesis, Massachusetts Institute of Technology (2011).
[39] J. Connor and H. Wilson, "A review of theories of the LH transition," Plasma Phys. and Control. Fusion **42**, R1 (2000).
[40] D. Whyte, A. Hubbard, J. Hughes, B. Lipschultz, J. Rice, E. Marmar, M. Greenwald, I. Cziegler, A. Dominguez, T. Golfinopoulos, *et al.*, "I-mode: an H-mode energy confinement regime with L-mode particle transport in Alcator C-Mod," Nuclear Fusion **50**, 105005 (2010).
[41] I. Cziegler, P. Diamond, N. Fedorczak, P. Manz, G. Tynan, M. Xu, R. Churchill, A. Hubbard, B. Lipschultz, J. Sierchio, *et al.*, "Fluctuating zonal flows in the I-mode regime in Alcator C-Mod)," Phys. Plasmas **20**, 055904 (2013).
[42] D. Auerbach, T. Carter, S. Vincena, and P. Popovich, "Resonant drive and nonlinear suppression of gradient-driven instabilities via interaction with shear Alfvén wavesa)," Phys. Plasmas **18**, 055708 (2011).
[43] X. Garbet, Y. Idomura, L. Villard, and T. Watanabe, "Gyrokinetic simulations of turbulent transport," Nuclear Fusion **50**, 043002 (2010).
[44] C. Holland, A. White, G. McKee, M. Shafer, J. Candy, R. Waltz, L. Schmitz, and G. Tynan, "Implementation and application of two synthetic diagnostics for validating simulations of core tokamak turbulence," Phys. Plasmas **16**, 052301 (2009).
[45] B. LaBombard and L. Lyons, "Mirror Langmuir probe: A technique for real-time measurement of magnetized plasma conditions using a single Langmuir electrode," Rev. Sci. Instrum. **78**, 073501 (2007).
[46] O. E. Garcia, S. M. Fritzner, R. Kube, I. Cziegler, B. LaBombard, and J. L. Terry, "Intermittent fluctuations in the Alcator C-Mod scrape-off layer)," Phys. Plasmas **20**, 055901 (2013).
[47] O. Garcia, I. Cziegler, R. Kube, B. LaBombard, and J. Terry, "Burst statistics in Alcator C-Mod SOL turbulence," Journal of Nuclear Materials **438**, S180–S183 (2013).
[48] R. Kube, A. Theodorsen, O. Garcia, B. LaBombard, and J. Terry, "Fluctuation statistics in the scrape-off layer of Alcator C-Mod," Plasma Phys. and Control. Fusion **58**, 054001 (2016).
[49] A. Theodorsen, O. Garcia, J. Horacek, R. Kube, and R. Pitts, "Scrape-off layer turbulence in TCV: evidence in support of stochastic modeling," Plasma Phys. and Control. Fusion **58**, 044006 (2016).
[50] O. Garcia, R. Kube, A. Theodorsen, J.-G. Bak, S.-H. Hong, H.-S. Kim, R. Pitts, and the KSTAR Project Team, "SOL width and intermittent fluctuations in KSTAR," arXiv preprint arXiv:1611.03440 (2016).
[51] O. E. Garcia and A. Theodorsen, "Power law spectra and intermittent fluctuations due to uncorrelated Lorentzian pulses," Phys. Plasmas **24**, 020704 (2017).